Journal of Alloys and Compounds 674 (2016) 245–251

Contents lists available at ScienceDirect

Journal of Alloys and Compounds

journal homepage: http://www.elsevier.com/locate/jalcom

Review

White photoluminescence emission from ZrO_2 co-doped with Eu^{3+}, Tb^{3+} and Tm^{3+}

L.X. Lovisa [a, *], V.D. Araújo [b], R.L. Tranquilin [c], E. Longo [c], M.S. Li [d], C.A. Paskocimas [a], M.R.D. Bomio [a], F.V. Motta [a]

[a] Departamento de Engenharia de Materiais, Universidade Federal do Rio Grande do Norte, 59072-970, Natal, RN, Brazil
[b] UACSA, Universidade Federal Rural de Pernambuco, 54510-000, Cabo de Santo Agostinho, PE, Brazil
[c] LIEC, Universidade Federal de São Carlos, 13565-905, São Carlos, SP, Brazil
[d] Instituto de Física de São Carlos, Universidade de São Paulo, 13566-590, São Carlos, SP, Brazil

ARTICLE INFO

Article history:
Received 9 August 2015
Received in revised form
2 March 2016
Accepted 7 March 2016
Available online 11 March 2016

Keywords:
Complex polymerization method
ZrO_2:RE^{3+}
Luminescence
CIE

ABSTRACT

The search for high efficiency, reliable, low power consumption and environmental friendly materials for white light-emitting diodes has become a proficient field. Single-phase doped materials have been made to solve some of these challenges. Particles with color-tunable emission can be obtained by a combination of some lanthanide ions in the host material. The luminescence properties and crystalline structure of ZrO_2 particles co-doped with rare earth ions (RE^{3+} = Tb^{3+}, Eu^{3+} and Tm^{3+}) calcined at different temperatures were studied. We aimed to investigate the emission spectrum of the particles in the red, green, and blue regions under UV excitation. The x and y coordination chromaticity - (x = 0.34, y = 0.34) and (x = 0.31, y = 0.34) - presented values close to those of the white color (x = y = 0.33). In conclusion, the ZrO_2:RE^{3+} powers were successfully obtained by the complex polymerization method and are promising candidates for white light-emitting applications.

Contents

1. Introduction

The incorporation of luminescent materials into host lattices, including transition metals and lanthanide ions, and their utilization has been reported by Blasse and Grabmaier [1]. Feldman and co-authors [2] have described numerous matrices with characteristic color emission and ending with the first use of the rare earth phosphors in the 1970s, including tricolor devices (RGB) containing lanthanide ions for application in white light emission based on f–f transition. Lanthanide doped particles have been recognized as a new promising class of fluorescent materials due to the unique luminescence properties, narrow line-width emission bands, high quantum yields and photostability [3]. Particles with color-tunable emission can be obtained by a combination of some lanthanide ions in the host material. Such a color-tunable phosphorus can find potential applications in display and security

* Corresponding author. Tel: +55 84 3342 2512; fax: +55 84 3342 2406.
E-mail address: lovisaengmat@ig.com.br (L.X. Lovisa).

http://dx.doi.org/10.1016/j.jallcom.2016.03.037
0925-8388/

printing areas [4].

Thulium, terbium, and europium are lanthanide ions that emit blue, green, and red color, respectively [5–12]. Many hosts can serve as promising matrices to accommodate these ions, yielding materials with efficient emission for application in tricolor white light-emitting devices [13–18]. Other lanthanides have also been used [19–25], but they have been incorporated separately or the excitation appears in a different wavelength.

Zirconia particles doped with different rare earths ions have been recognized to have potential in the area of photonic applications [26–28]. The low-phonon energy of ZrO_2 opens up the possibility of more efficient luminescence from the activator ions incorporated in it [29]. This is due to the fact that the lower the phonon energy of the host, the higher the probability of radiative transitions of RE^{3+}. The energy phonon and symmetries of the normal modes of vibration of the ZrO_2 are determined as a function of crystalline structure [30,31]. According to Negita [32], in his study lattice vibrations and cubic to tetragonal phase transition in ZrO_2, shows through of analyzes of phonon modes in ZrO_2 that there is a condensation of the phonon X_2^- associated with the cubic phase to tetragonal transition in ZrO_2.

Zirconium dioxide is an excellent material for optical application due to its hardness, optical transparency and high refractive index. Zirconia coatings due to its chemical and photochemical stability, high refractive index and low phonon energy seem to be an ideal material for preparation of active wave guides [33]. The wide band gap of ZrO_2 enables RE emission in the visible range, as low phonon energies of the matrix suggest a high yield luminescence (multiphonon relaxation). The luminescence spectrum of lanthanides in the trivalent state caused by ionization of $6s^2$ and 5d electrons and intracenter transitions of 4f electrons shielded by outer 5s and 5p electrons consists of a set of fairly narrow spectral lines from the UV to the IR range [34,35].

Thus, rare earth ion doped ZrO_2 can be a good choice as phosphor materials for white light-emitting UV-LEDs. Recently, the luminescence properties of $Eu^{3+}/Dy^{3+}/Tm^{3+}$ activated ZrO_2 nanocrystals have been reported [36–38]. These rare earth ion doped ZrO_2 nanophosphors have been reported to give multicolor emissions.

In this paper, we used photoluminescence spectroscopy to investigate the white light emission of ZrO_2 particles co-doped with rare earth ions (RE^{3+} = Tb^{3+}, Eu^{3+} and Tm^{3+}). The samples were prepared by the complex polymerization method (CPM) [39–41] and characterized by XRD and diffuse reflectante spectroscopy.

2. Experimental

2.1. Synthesis of ZrO_2:RE particles

The samples were prepared by a Complex Polymerization Method (CPM) [42,43]. In the process of synthesis, zirconium citrate was obtained by dissolution of zirconium nitrate (Vetec, 99%) in an aqueous citric acid solution under agitation at an approximate temperature of 80 °C. After the complete dissolution of zirconium nitrate, the cations of RE were added for doping. A europium solution and a thulium solution were prepared through the dissolution of Eu_2O_3 (Aldrich, 99.9%) and Tm_2O_3 (Aldrich, 99.9%), respectively, in nitric acid. Then, the solutions were mixed with the zirconium citrate solution. Terbium nitrate was added (Aldrich, 99.9%). In order to promote the polymerization of citrate through the polyesterification reaction, ethylene glycol was added, and the solution was stirred constantly. The molar ratio between citric acid and ethylene glycol was set to 60/40 (mass ratio). After 4 h, the removal of water and the formation of translucent resin was observed. The dopant concentration was maintained at 8 mol% RE, this content is the contribution of all RE, corresponding to ZrO_2: 2.66% Tm 2.66% Tb 2.68% Eu. The polymeric resin was heat treated at 350 °C (10 °C/min) for 4 h, leading to the partial decomposition of the polymeric gel and the formation of an expanded resin composed of partially pyrolyzed material. The particles were annealed at 600, 800 and 1000 °C for 2 h at a heating rate of 10 °C/min.

2.2. Characterization of ZrO_2:RE particles

The phases present in the ceramic powder were investigated by X-ray diffraction (XRD) using a Shimadzu diffractometer, model XRD-7000, with CuKα radiation. Raman spectrometry required use of Horiba Jobin-Yvon Raman Labram equipment at room temperature as the source of excitation by means of an Olympus BX41 TM microscope with a laser at a wavelength of 514 nm, in the 100–700 nm. The UV–vis reflectance spectra of the ZrO_2: 8%RE particles were measured using Cary equipment, model 5G, in the 200–800 nm range. Photoluminescence spectra were obtained using a Thermal Jarrell-Ash Monospec 27 monochromator and Hamamatsu R446 photomultiplier. The excitation source used on the samples was a laser at a wavelength of 350.7 nm with krypton ions (Coherent Innova) with an output of approximately 13.3 mW; all measurements were performed at room temperature. To characterize white light resulted from the described mixing, we calculated the chromaticity coordinates using the spectrum represented in Fig. 3. The chromaticity coordinates of red (the x coordinate), green (the y coordinate) and blue (the z coordinate) were determined according to the system of the International Commission on Illumination given in 1968 [44,45] using the following relationships:

$$x = \frac{(X)}{(X+Y+Z)} \quad y = \frac{(Y)}{(X+Y+Z)} \quad z = \frac{(Z)}{(X+Y+Z)} \tag{1}$$

where parameters X, Y and Z are the following spectral integrals:

$$X = \int xP(\lambda)d\lambda \quad Y = \int yP(\lambda)d\lambda \quad Z = \int zP(\lambda)d\lambda \tag{2}$$

Here P(λ) is luminescence spectrum of the samples, that provide, for each within the visible range, the emitted intensity. The function P(λ) is determined empirically, the values of λ for components *x*, *y* and *z* are 599, 555 and 446 nm, respectively [46] and *x*, *y* and *z* are functions of spectral summarizing. Integrals (2) were calculated through the spectral interval of 350–800 nm.

3. Results and discussion

The XRD patterns of ZrO_2: 8%RE samples calcined at different temperatures are shown in Fig. 1a. Diffraction peaks are located at approximately 29.94°, 34.75°, 49.87°, 59.43°, 62.45° and 73.66°, which correspond to the (111), (200), (220), (311), (222), and (400) planes, respectively, of cubic ZrO_2 phase [ICSD 81-1551]. According to the literature [47,48], stabilization of the cubic phase of ZrO_2 is achieved by increasing the amount of bi- or trivalent cations introduced into the ZrO_2 structure. The replacement of cations of Zr^{4+} by RE^{3+} promotes the appearance of oxygen vacancies (Vo). The oxygen vacancies are responsible for weakening the repulsive force between neighboring O^{2-} and results in a change in the lattice parameters of the unit cell (c/a → 1), which causes the ions to be arranged in a cubic structure [47].

The identification of the crystalline phase of ZrO_2 by only XRD is inaccurate due to the polymorphism of ZrO_2. This difficulty is reported by Das el at [48] which in his work confirms an inaccuracy in

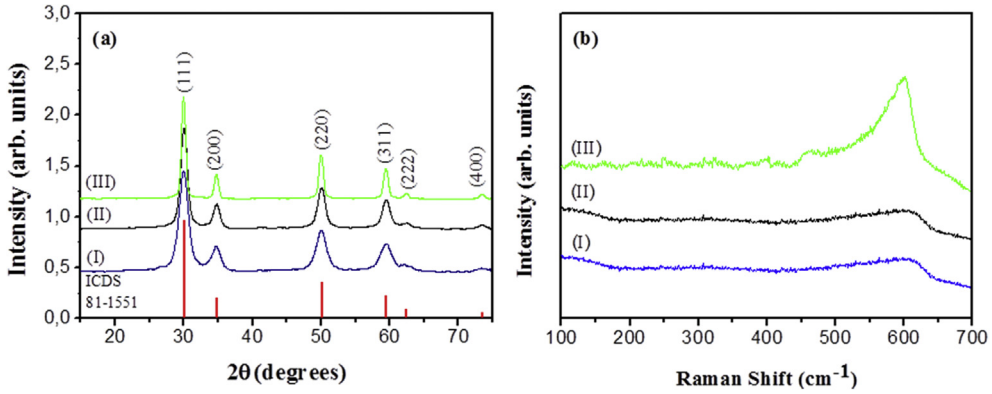

Fig. 1. (a) Diffraction pattern of ZrO_2:RE samples, (b) Raman spectrum of ZrO_2:RE samples, calcined at different temperatures: (I) 600 °C, (II) 800 °C and (III) 1000 °C.

Table 1
Value of structural parameters of ZrO_2:RE particles.

Treatment temperature	Crystal system	Space group	2θ	FWHM (rad)	Lattice parameter: a (Å)	Unit cell volume (Å^3)	Crystallite size (nm)
T: 600 °C	Cubic	Fm-3m	29.9	0.82	5.1504	136.6	13.2
T: 800 °C	Cubic	Fm-3m	29.9	0.49	5.1524	136.8	13.5
T: 1000 °C	Cubic	Fm-3m	29.9	0.3149	5.1579	137.2	17.9

identifying the tetragonal and cubic phases by XRD due to low angular resolution of the equipment used (0.03°), assuming an overlap of peaks of the two phases of ZrO_2. Raman spectroscopy can distinguish modifications of the crystalline structure of ZrO_2 with higher efficiency [49]. The analysis is based on the different vibrations that each crystalline structure of ZrO_2 has. The Raman spectra of oxide ceramics typically contain a large amount of information that is extracted from the band positions, their intensities, and their shapes.

The Raman spectrum of the sample treated at different temperatures is shown in Fig. 1b. The spectrum shows a single band centered at between 600 cm^{-1}. This band is associated to the T_{2g} characteristic vibration of the cubic phase of ZrO_2 [49]. Kontoyannis and Orkoula [49], in his study of the quantitative determination of the phases of ZrO_2, show quite clearly the distinct behavior in Raman spectra between the tetragonal and cubic phases. To tetragonal phase are assigned six active raman modes ($A_{1g} + 2B_{1g} + 3E_g$), for the cubic phase have only one mode (T_{2g}). The results for the raman confirm the response obtained by XRD: stabilization of cubic phase [50].

Crystallite size of the samples was estimated by the Scherrer equation and the full-width half-maximum (FWHM) of an observed peak. The strongest peaks for the cubic phase (111) were used to calculate the average crystallite size (D) of the ZrO_2:RE particles. Table 1 gives the lattice parameters (a), unit cell volume (V), and crystallite size for the ZrO_2: 8%RE samples.

A significant reduction in the FWHM value with increasing temperature is observed from Table 1. This behavior indicates that there was an increase in crystallinity with temperature effect. Samples presented small crystallite size ranging from 13.2 to 17.9 nm. Crystallite size of the samples was estimated by the Scherrer equation and the full-width half-maximum (FWHM) of an observed peak. The strongest peaks for the cubic phase (111) were used to calculate the average crystallite size (D) of the ZrO_2:RE particles. Table 1 gives the lattice parameters (a), unit cell volume (V), and crystallite size for the ZrO_2: 8%RE samples.

The band gap energies of the ZrO_2: 8%RE nanoparticles were estimated from their diffuse reflectante spectroscopy by plotting the square of the Kubelka–Munk function $F(R)^2$ vs. energy in electron volts and extrapolating the linear part of the curve to $F(R)^2 = 0$, as shown in Fig. 2. The ratio between the molar absorption coefficient (k) and scattering coefficient (s) is estimated from reflectance data using the Kubelka–Munk relation [51] in Equation (3):

$$F(R) = \frac{k}{s} = \frac{(1-R)^2}{2R} \quad (3)$$

where R is the percentage of reflected light. The incident photon energy ($h\nu$) and the optical band gap energy (Eg) are related to the transformed Kubelka–Munk function, $[F(R)\ h\nu]^p = A(h\nu - Eg)$, where Eg is the band gap energy, A is a constant depending on the transition probability and p is the power index that is related to the optical absorption process. p equals to 1/2 or 2 for an indirect or a direct allowed transition, respectively.

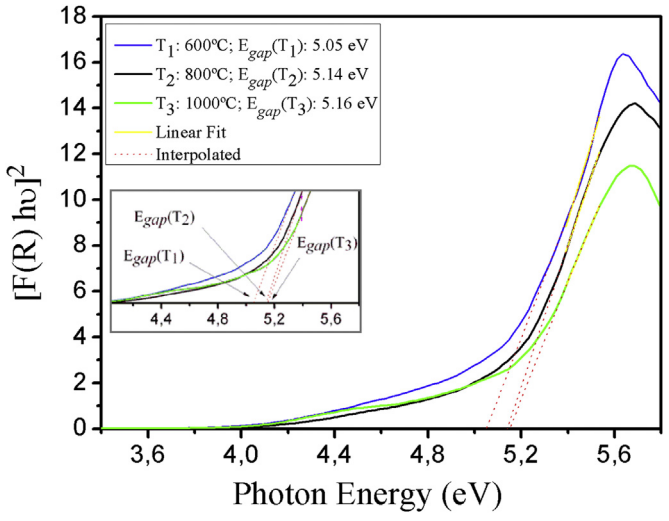

Fig. 2. UV–vis absorption spectroscopy of ZrO2:RE particles thermally treated at 600 °C, 800 °C and 1000 °C.

Table 2
Comparative results between optical band gap values of ZrO_2: 8%RE obtained in this work with those reported in the literature for doped ZrO_2 obtained by different methods.

Material	Method employed	Temperature (°C)	Concentration of dopant (mol %)	Optical band gap (eV)	Ref. []
ZrO_2:Ce	Microwave irradiation	400	5	3.84	[53]
			10	3.79	
			15	3.75	
ZrO_2:Au (films)	Sol–gel dip coating	500	4	5.71	[54]
			8	5.70	
			10	5.64	
			12	5.40	
ZrO_2: Eu	Combustion	400	1	4.70	[55]
			3	4.60	
			5	4.50	
			7	4.40	
			9	4.30	
			11	4.20	
ZrO_2: Mg (films)	Sol–gel	500	4	5.69	[56]
			8	5.59	
			12	5.44	
			16	5.14	
			20	4.42	
ZrO_2:RE	CPM	600	8	5.05	This work
		800		5.14	
		1000		5.16	

The calculated values of band gap E_{gap} were listed in Fig. 2. The spectra behavior shows that the E_{gap} is dependent of heat treatment temperature. This result indicates that the exponential optical absorption edge and optical band gap are controlled by the degree of structural defects into the lattice. Thus, the increase of optical band gap value with the heat treatment temperature promotes a reduction of the intermediary energy levels, as consequence of the structural organization in the lattice [52].

Table 2 shows a comparative between E_{gap} values of ZrO_2: 8%RE prepared by CPM with those reported in the literature for the doped ZrO_2 particles prepared by different methods [53–56].

In this table, it was verified that the E_{gap} of ZrO_2 can be influenced by the formation methods. Also, there has been a change in the gap energy values is a function of the type and amount of dopant introduced in the ZrO_2 lattice.

According to band theory, the energy of a forbidden band is dependent on material structure since the changing of atom positions lead to changing of the integral of exchange interaction. This is the reason for forbidden band energy dependence on the ZrO_2 crystal structure (monoclinic, tetragonal and cubic). The experimentally estimated forbidden gap for monoclinic phase is 4.2–5.83 eV, for tetragonal 4.2–5.78 and for cubic 4.6–6.1 eV [57,58]. The theoretically calculated forbidden gap for monoclinic phase is 4.46 eV, for tetragonal phase is 4.28 eV and for cubic phase is 4.93 eV [57,58].

Table 3
Assignments of the rare earth ions transitions and the respective wavelength.

Peaks	Transitions	Wavelength (nm)
1	$^1G_4 \rightarrow {}^3H_6$ (Tm^{3+})	466
2	$^5D_4 \rightarrow {}^7F_6$ (Tb^{3+})	495
3	$^5D_4 \rightarrow {}^7F_6$ (Tb^{3+})	550
4	$^5D_0 \rightarrow {}^7F_1$ (Eu^{3+})	596
5	$^5D_0 \rightarrow {}^7F_2$ (Eu^{3+})	619
6	$^5D_0 \rightarrow {}^7F_3$ (Eu^{3+})	656
7	$^5D_0 \rightarrow {}^7F_4$ (Eu^{3+})	706

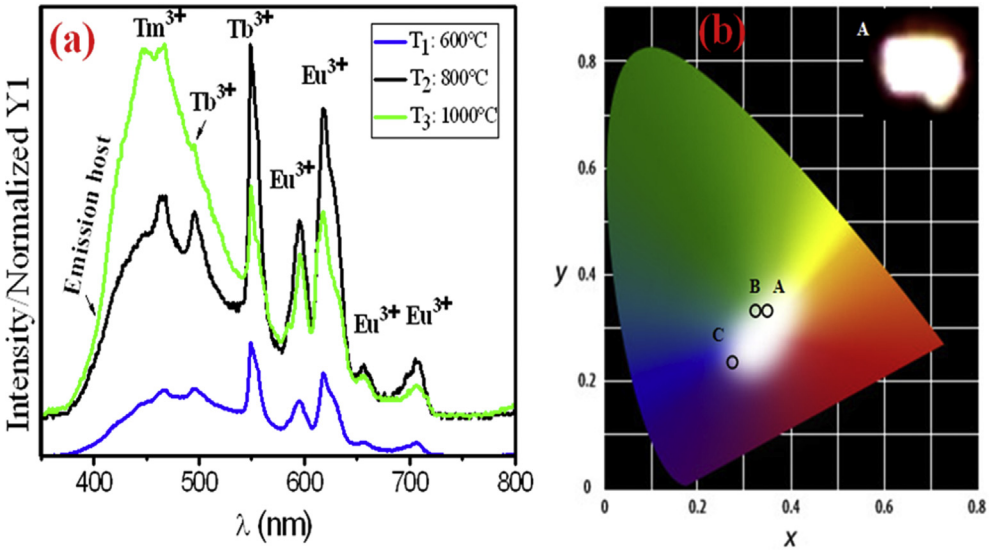

Fig. 3. (a) PL emission of ZrO_2:E to temperature at 600, 800 e 1000 °C; (b) CIE diagram of ZrO_2:RE, A: 600 °C, B: 800 °C, C: 1000 °C. Inset shows emission light white of the sample A.

The emission spectra of the ZrO_2: 8%RE excited at 350.7 nm (Fig. 3a) presented the peaks ascribed to the lanthanides ions Tm^{3+}, Tb^{3+} and Eu^{3+}. The peak detected at 466 nm (blue region) corresponds to the Tm^{3+} $^1G_4 \rightarrow {}^3H_6$ transition [59]; it had a different relative intensity in each spectrum. The peaks at 495 and 550 nm (green region) refer Tb^{3+} $^5D_4 \rightarrow {}^7F_6$ and $^5D_4 \rightarrow {}^7F_5$ transitions [60], respectively. The ones relative to the Eu^{3+} $^5D_0 \rightarrow {}^7F_j$ (1, 2, 3 and 4) transitions [61] appeared at 596, 619, 656 and 706 nm (region red), respectively. Table 3 lists the transitions we observed in Fig. 3.

Owing to the different charge for the cations, oxygen vacancies were formed to balance the charge difference. The defect reaction equation can be described in the following Eq. (4):

$$(1-x)ZrO_2 + 1/2xRE_2O_3 \rightarrow xRE'_{Zr} + 1/2xV''_o + (1-x)Zr^x_{Zr} + (2-1/2x)O^x_o \quad (4)$$

where RE_{Zr}, means RE^{3+} occupying the normally occupied by a Zr^{4+} due to replacement by RE^{3+}. V''_o is the O^{2-} vacancy. Zr^x_{Zr} represents the rest zirconium in the lattice of ZrO_2 and O^x_o is the oxygen in the lattice of ZrO_2. At low concentrations of RE, there is little V''_o in ZrO_2, and the symmetry of the host structure is not seriously influenced. The larger the concentration of RE in the host, higher the number of oxygen vacancies is able to create a new surrounding in the host. The new surrounding disturbs the symmetry of the host.

It is observed in Fig. 3 that increasing crystallinity favored obtaining a better answer of photoluminescence. Emissions of Eu^{3+} $^5D_0 \rightarrow {}^7F_j$ (j = 1, 2) can be caused by the direct activation of photon or through energy transfer of Tb^{3+} [donor (Tb^{3+}) → receptor (Eu^{3+})]. It is known that the photoluminescence is dependent on the degree of order-disorder of the material; so this property follows the structural evolution of the material.

Table 4
CIE coordinates of ZrO_2: 8%RE; A: 600 °C, B: 800 °C, C: 1000 °C.

Sample	x	y
A	0.34	0.34
B	0.31	0.34
C	0.28	0.24

The spectrum presents a broad band between 378 nm and 572 nm, associated with the interference of the host. Generally, the photoluminescent is related to defects and/or impurities found on the lattice [62–65]. The structural defects of ZrO_2 in most are related to O^{2-} and Zr^{4+} vacancies. The formation of these defects can be described through the Equations (5), (6) and (7) [66]:

$$ZrO_2 + h\nu \rightarrow Zr^{4+} + O_2 + 4e^- \quad (5)$$

$$Zr^{4+} + e^- \rightarrow Zr^{3+} \quad (6)$$

$$2O_o \rightarrow 2V_o^{2+} + O_2 + 4e^- \quad (7)$$

Zr^{4+} ions may generate Zr^{3+} centers by capturing electrons. The O_0 represents an oxygen atom in a regular position in the lattice, V_0 indicates an oxygen vacancy. The oxygen vacancy always leads to formation of energy levels within the band gap. When ZrO_2 is excited by a photon, the electrons are trapped by V_0 and centers are created (F) [67]. Then recombination centers (F) with the holes (h^+) creates the transmitter excited states. From these states originate transitions which decay to a state with lower energy level. Wang et al. [68] analyzed the effect on temperature treatment between 600 °C e 1550 °C on ZrO_2 photoluminescence behavior. It was observed a gradual growth of the PL intensity until the temperature of 1100 °C and surprisingly, from 1200 °C was verified a very rapid growth of the PL intensity. According to authors, at high temperature the diffusion of various species present in the material is favored, as the case of the oxygen vacancy. The quantity of oxygen vacancies tend to gradually increase with increasing treatment temperature and, therefore, the emissions due to recombination centers also grow. For the sample treated at 1000 °C, the ZrO_2 matrix shows a significant contribution in the blue region, favored by increasing the treatment temperature. It is observed that on this last case, the energy transfer between ZrO_2 → RE^{3+} [36] was not effective, which clarifies the decrease in emissions intensity of Tb^{3+} (548.32 nm) and Eu^{3+} (617.54 nm).

The white emission can be verified by determining the coordinates x and y. The CIE chromatic coordinates can be calculated by integration of the X, Y, and Z values [69]. Fig. 3b illustrates the

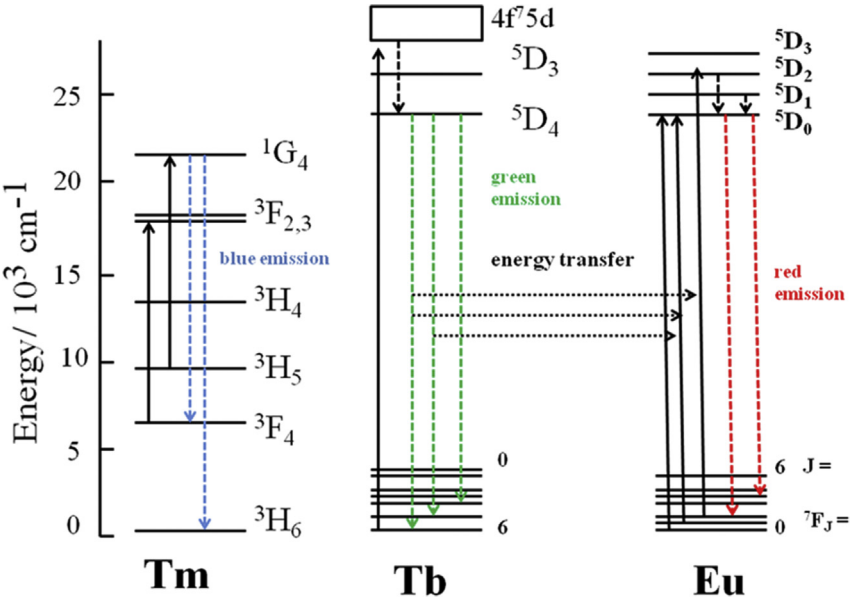

Fig. 4. The energy transfer mechanism scheme between the ions $Tm^{3+}/Tb^{3+}/Eu^{3+}$.

CIE chromaticity diagram. The standard white light presents x = 0.33 and y = 0.33 [70]. Table 4 lists the chromaticity coordinates for ZrO_2: 8%RE excited at 350.7 nm. The contributions from certain emission regions define the color of the matrix. The samples treated at 600 °C and 800 °C represented by letters A and B, respectively, show white emission as illustrated in Fig. 3b. It is observed in the inset in Fig. 3, white light-emission for sample calcined at 600 °C under Uv excitation. The sample treated at 1000 °C, identified by letter C, presented violet color.

It has been recognized that the luminescence intensities of various rare earth ions can be enhanced or quenched by the energy transfer from other codoped rare earth ions. The energy transfer (ET) between Tb^{3+} and Eu^{3+} in nanopowder has been widely studied to understand its photoluminescent behavior [71, 72].

A schematic energy level diagram involving Tm^{3+}, Tb^{3+}, and Eu^{3+} absorption; nonradiative relaxation; and processes leading to the blue, green, and red emission is given in Fig. 4.

Fig. 4 shows that no resonant energy transfer process from the $^5D_4$ state of Tb^{3+} to $^5D_0$ of Eu^{3+} can occur. The most probable mechanisms responsible for the direct transfer of excitation are:

$$^5D_4(Tb) + {}^7F_0(Eu) + \Delta E(1) \rightarrow {}^7F_4(Tb) + {}^5D_0(Eu) \quad (8)$$

$$^5D_4(Tb) + {}^7F_1(Eu) \rightarrow {}^7F_4(Tb) + {}^5D_0(Eu) + \Delta E(2) \quad (9)$$

where the energy mismatches ΔE(1) and ΔE(2) can be bridged respectively by the absorption or the emission of the phonons or by the involvement of energy levels of other ions in a many-body process. Further information about the mechanism responsible for the transfer can be obtained from the analysis of the kinetics of the luminescence as a function of the fractional concentration x and of the temperature.

First, electrons in Tb^{3+} ions are excited from the ground state ($4f^8$) to the excited state ($4f^75d$) by 350.7-nm UV light. Subsequently, these electrons relax to the lowest excited state, $^5D_4$, through multiphonon relaxation and then either return to the ground state to produce the Tb^{3+} emissions ($^5D_4 \rightarrow {}^7F_{6,\ 5,\ 4}$) or transfer their excitation energy from the $^5D_4$ (Tb^{3+}) level to the higher excited energy levels of Eu^{3+} ($4f^6$) through cross relaxation, in which they relax to the $^5D_0$ (Eu^{3+}) level, where red-orange emission ($^5D_0 \rightarrow {}^7F_{0,\ 1,\ 2}$) occurs. Because the $^5D_4 \rightarrow {}^7F_{6,\ 5,\ 4,\ 3}$ emissions of Tb^{3+} effectively overlap with the $^7F_{0,\ 1} \rightarrow {}^5D_{0,\ 1,\ 2}$ absorptions of Eu^{3+}, the energy transfer from Tb^{3+} to Eu^{3+} is very efficient in general.

4. Conclusion

ZrO_2: 8%RE particles were successfully obtained by the complex polymerization method. Through XRD analysis, the phase identified in ZrO_2: 8%RE was the cubic phase. The photoluminescence emission spectra show transitions of the type $^1G_4 \rightarrow {}^3H_6$ (466 nm) from Tm^{3+}, $^5D_4 \rightarrow {}^7F_{5,6}$ (495 nm and 550 nm) from Tb^{3+}, and $^5D_0 \rightarrow {}^7F_{1,2}$ (597, 619, 656 and 706 nm) from Eu^{3+}. Energy transfer was observed between levels $^5D_4$ (Tb^{3+}) → $^5D_1$ (Eu^{3+}). The CIE coordinates calculated for particles treated at 600 °C and 800 °C showed values of (x = 0.34, y = 0.34) and (x = 0.31, y = 0.34), respectively; according to the CIE diagram, the values represent a points in the white region. The ZrO_2:RE materials presented here are promising photoluminescent materials for applications in new white light-emitting devices.

Acknowledgment

The authors gratefully acknowledge the financial support of the Brazilian governmental research funding agencies CAPES, CNPq, FAPESP 2013/07296-2 and INCTMN 2008/57872-1.

References

[1] G. Blasse, B. Grabmaier, Luminescent Materials, Springer Verlag, Berlin Heidelberg, 1994.
[2] C. Feldman, T. Justel, C.R. Ronda, P.J. Schmidt, Inorganic luminescent materials: 100 years of research and application, Adv. Funct. Mater 13 (2003) 511–516.
[3] Y. Wang, R.X. Yan, Z.Y. Hao, L. Wang, J.H. Zeng, H. Bao, X. Wang, Q. Peng, Y.D. Li, Fluorescence resonant energy transfer biosensor based on upconversion-luminescent nanoparticles, Angew. Chem. Int. Ed. 44 (2005) 6054–6057.
[4] T.S. Atabaev, Y.-H. Hwang, H.-K. Kim, Color-tunable properties of Eu^{3+}- and Dy^{3+}-codoped Y_2O_3 phosphor particles, Nanoscale Res. Lett. 7 (2012) 556–563.
[5] E.A. Morais, L.V.A. Scalvi, A. Tabata, J.B.B. De Oliveira, S.J.L. Ribeiro, Photoluminescence of Eu^{3+} ion in SnO_2 obtained by sol–gel, J. Mater Sci. 43 (2008) 345–349.
[6] L. Gao, Y. An, H. Zhu, L. Wang, J. Chen, N. Wang, Hydrothermal synthesis and photoluminescence properties of $Y_2Zr_2O_7$:Tb^{3+} phosphors, J. Mater Sci. 46 (2011) 1337–1340.
[7] R. Krishna, D. Haranath, S.P. Singh, H. Chander, A.C. Pandey, D. Kanjilal, Synthesis and improved photoluminescence of Eu:ZnO phosphor, J. Mater Sci. 42 (2007) 10047–10051.
[8] S. Sailaja, S.J. Dhoble, N. Brahme, B.S. Reddy, Synthesis, structural, photoluminescence and mechanoluminescence properties of Tb^{3+}: $Ca_2Gd_2W_3O_{14}$ novel green nanophosphors, J. Mater Sci. 47 (2012) 2359–2364.
[9] D. Jin, X. Yu, X. Xu, L. Wang, N. Wang, Hydrothermal synthesis of amorphous spherical-shaped YBO_3:Eu^{3+} and its photoluminescence property, J. Mater Sci. 44 (2009) 6144–6148.
[10] W. Ma, X. Dong, J. Wang, W. Yu, G. Liu, Electrospinning preparation of LaOBr: Tb^{3+} nanostructures and their photoluminescence properties, J. Mater Sci. 48 (2013) 2557–2565.
[11] H. Wang, J. Yu, J. Li, X. Cheng, Z. Huang, The room temperature photoluminescence properties of Eu^{3+}-doped bi-phase calcium phosphate under visible light,, J. Mater Sci. 45 (2010) 1237–1241.
[12] X. Zhang, Z. Zhao, J. Chaudhuri, In-situ crystal growth and photoluminescence properties of YBO_3: Tb^{3+} microstructures, J. Mater Sci. 50 (2015) 251–257.
[13] H. Zhang, X. Fu, S. Niu, Q. Xin, Blue emission of ZrO_2:Tm nanocrystals with different crystal structure under UV excitation, J. Non-Cryst. Solids 354 (2008) 1559–1563.
[14] V.H. Romero, E. De la Rosa, P. Salas, J.J. Velázquez-Salazar, Strong blue and white photoluminescence emission of $BaZrO_3$ undoped and lanthanide doped phosphor for light emitting diodes application, J. Solid State Chem. 196 (2012) 243–248.
[15] K.V.R. Murthy, A.S. Prasad, M.R. Rao, Luminescence Characteristics of Eu and Tb Doped $YGdBO_3$ Phosphor, Phys, Procedia 29 (2012) 70–75.
[16] P.C. De Sousa, O.A. Serra, Red, green, and blue lanthanum phosphate phosphors obtained via surfactant-controlled hydrothermal synthesis, J. Lumin 129 (2009) 1664–1668.
[17] J. Hao, S.A. Studenikin, M. Cocivera, Blue, green and red cathodoluminescence of Y_2O_3 phosphor films prepared by spray pyrolysis, J. Lumin 93 (2001) 313–319.
[18] C.-J. Zhao, J.-L. Cai, R. Li, S.-L. Tie, X. Wan, J.-Y. Shen, A Dy^{3+}-doped $LiYF_4$ single crystal capable of generating white light,, J. Non-Cryst. Solids 358 (2012) 604.
[19] M.A. Zaitoun, S. Al-Tarawneh, Effect of varying lanthanide local coordination sphere on luminescence properties illustrated by selected inorganic and organic rare earth complexes synthesized in sol–gel host glasses, J. Lumin 131 (2011) 1795–1801.
[20] I. Sabikoglu, M. Ayvacýklý, A. Bergeron, A. Ege, N. Can, Photoluminescence investigations of Li_2SiO_3:Ln (Ln=Er^{3+}, Eu^{3+}, Dy^{3+}, Sm^{3+}) phosphors, J. Lumin 132 (2012) 1597–1602.
[21] S. Hu, J. Yang, C. Li, J. Lin, Synthesis and up-conversion white light emission of RE^{3+}-doped lutetium oxide nanocubes as a single compound, Mater. Chem. Phys. 133 (2012) 751–756.
[22] Z. Hou, C. Li, P. Ma, Z. Cheng, X. Li, X. Zhang, Y. Dai, D. Yang, H. Lian, J. Lin, Up-Conversion Luminescent and Porous $NaYF_4$:Yb^{3+}, Er^{3+}@SiO_2Nanocomposite Fibers for Anti-Cancer Drug Delivery and Cell Imaging, Adv. Funct. Mater 22 (2012) 2713–2722.
[23] M. Ayvacikli, A. Ege, N. Can, Radioluminescence of $SrAl_2O_4$:Ln^{3+}(Ln = Eu, Sm, Dy) phosphor ceramic, Opt. Mater 34 (2011) 138–142.
[24] S.-A. Yan, J.-W. Wang, Y.-S. Chang, W.-S. Hwang, Y.-H. Chang, Synthesis and luminescence properties of Ln^{3+} (Ln^{3+} = Er^{3+}, Sm^{3+})-doped barium lanthanum tungstate $BaLa_2WO_7$ phosphors, Opt. Mater 34 (2011) 147–151.
[25] R. Kumar, M. Nyk, T.Y. Ohulchanskyy, C.A. Flask, P.N. Prasad, Combined optical and MR bioimaging using rare earth ion doped $NaYF_4$ nanocrystals, Adv. Funct. Mater 19 (2009) 853–859.
[26] R. Yan, Y. Li, Down/Up Conversion in Ln^{3+}-Doped YF_3, Nanocrystals, Adv. Funct. Mater 15 (2005) 763.
[27] E. De la Rosa-Cruz, L.A. Diaz-Torres, P. Salas, R.A. Rodrıguez, G.A. Kumar, M.A. Meneses, J.F. Mosiño, J.M. Hernández, O. Barbosa-Garcia, Luminescent properties and energy transfer in ZrO_2: Sm^{3+} nanocrystals, J. Appl. Phys. 94 (2003) 3509–3515.
[28] Z. Assefa, R.G. Haire, P.E. Raison, Correlation of the oxidation state as cerium in

sol-gel glasses as a function of thermal treatment via optical and XANES studies, Spectrochim. Acta A 60 (2004) 89–95.
[29] P. Salas, C. Angeles, J.A. Montoya, E. De la Rosa, L.A. Dıaz-Torres, A. Martınez, M.A. Romero-Romo, J. Morales, Synthesis, characterization and luminescence properties of ZrO_2: Yb^{3+}–Er^{3+} nanophosphor, Opt. Mater 27 (2005) 1295–1300.
[30] X. Zhao, D. Vanderbilt, Phonons and lattice dielectric properties of zirconia, Phys. Rev. B 65 (2002) 075105.
[31] A. Feinberg, C.H. Perry, Structural disorder and phase transitions in ZrO_2:Y_2O_3 system, J. Phys. Chem. Solids 42 (1981) 513–518.
[32] K. Negita, Lattice vibrations and cubic to tetragonal phase transition in ZrO_2, Acta Metall. 37 (1989) 313–317.
[33] R. Reisfeld, M. Zelner, A. Patra, Fluorescence study of zirconia films doped by Eu^{3+}, Tb^{3+} and Sm^{3+} and their comparison with silica films, J. Alloys Compd 300–301 (2000) 147–151.
[34] S. Cotton, Lanthanide and Actinide Chemistry, John Wiley & Sons, Ltd., Chichester, UK, 2006.
[35] I.S. Molchan, N.V. Gaponenko, R. Kudrawiec, J. Misiewiec, L. Bryja, G.E. Thompson, P. Skeldon, Visible luminescence from europium-doped alumina sol–gel derived films confined in porous anodic alumina, J. Alloys Compd. 341 (2002) 251.
[36] E. De la Rosa, L.A. Diaz-Torres, P. Salas, R.A. Rodrıguez, Visible light emission under UV and IR excitation of rare earth doped ZrO_2 nanophosphor, Opt. Mater 27 (2005) 1320.
[37] A. Mondal, S. Ram, Enhanced phase stability and photoluminescence of Eu^{3+} modified t-ZrO_2 nanoparticles, J. Am. Ceram. Soc. 91 (2008) 329–332.
[38] L.A. Diaz-Torres, E. De la Rosa, P. Salas, V.H. Romero, C. Angeles-Chavez, Efficient photoluminescence of Dy^{3+} at low concentrations in nanocrystalline ZrO_2, J. Solid State Chem. 181 (2008) 75–80.
[39] V.H. Romero, E. De la Rosa, T. López-Luke, P. Salas, C. Angeles-Chavez, Brilliant blue, green and orange–red emission band on Tm^{3+}-, Tb^{3+}- and Eu^{3+}-doped ZrO_2 nanocrystals, J. Phys. D. 43 (2010) 465105.
[40] P.N. Medeiros, V.D. Araujo, A.P.A. Marques, R.L. Tranquilin, C.A. Paskocimas, M.R.D. Bomio, J.A. Varela, E. Longo, F.V. Motta, Effect of different starting materials on the synthesis of $Ba_{0.8}Ca_{0.2}TiO_3$, J. Adv. Ceram. 4 (2015) 65–70.
[41] V.D. Araújo, F.V. Motta, A.P.A. Marques, C.A. Paskocimas, M.R.D. Bomio, E. Longo, J.A. Varela, Effect of calcium on the structural properties of $Ba_{(1-x)}Ca_xTiO_3$ particles synthesized by complex polymerization method, J. Mater Sci. 49 (2014) 2875–2878.
[42] F.V. Motta, A.P.A. Marques, J.W.M. Espinosa, P.S. Pizani, E. Longo, J.A. Varela, Room temperature photoluminescence of BCT prepared by Complex Polymerization Method, Curr. Appl. Phys. 10 (2010) 16–20.
[43] F.V. Motta, A.T. De Figueiredo, V.M. Longo, V.R. Mastelaro, A.Z. Freitas, L. Gomes, N.D. Vieira Jr., E. Longo, J.A. Varela, Disorder-dependent photoluminescence in $Ba_{0.8}Ca_{0.2}TiO_3$ at room temperature, J. Luminescence 129 (2009) 686–690.
[44] E.F. Schubert, Light Emitting Diodes, Cambridge University Press, 2003.
[45] R. Robertson, Computation of correlated color temperature and distribution temperature, J. Opt. Soc. Am. 58 (1968) 1528–1535.
[46] L.F. Santos, C.J. Pereira, Color composition by radiometric and photometric calibration of LEDs: Theory and experimente, Rev. Bras. Ensino Física 35 (2013) 2314.
[47] N. Shibata, J. Katamura, A. Kuwabara, Y. Ikuhara, T. Sakuma, The instability and resulting phase transition of cubic zirconia, Materials Science and Engineering A 312 (2001) 90–98.
[48] S. Das, C.-Y. Yang, C.-H. Lu, Structural and Optical Properties of Tunable Warm-White Light-Emitting ZrO_2:Dy^{3+} Eu^{3+} Nanocrystals, J. Am. Ceram. Soc. 96 (2013) 1602–1609.
[49] C.G. Kontoyannis, M. Orkoula, Quantitative determination of the cubic, tetragonal and monoclinic phases in partially stabilized zirconias by Raman spectroscopy, J. Mater Sci. 29 (1994) 5316–5320.
[50] V.G. Keramidas, W.B. White, Raman Scattering Study of Crystallization and Phase Transformation of ZrO2, J. Am. Ceram. Soc. 57 (1974) 22–24.
[51] P. Kubelka, F. Munk-Aussig, Ein beitrag zur optick der farbanstriche, Zeitschrift fur technische, Physik 12 (1931) 593–601.
[52] M.D. Gonçalves, L.S. Cavalcante, J.C. Sczancoski, J.W.M. Espinosa, P.S. Pizani, E. Longo, I.L.V. Rosa, (Sr,Tm)ZrO_3 powders prepared by the polymeric precursor method: Synthesis, optical properties and morphological characteristics, Opt. Mater. 31 (2009) 1134–1143.
[53] K. Gnanamoorthi, et al., Effect of Ce doping on microstructural, morphological and optical properties of ZrO_2 nanoparticles, Mater. Sci. Semicond. Process. 30 (2015) 518–526.
[54] J. Berlin, K. Joy, Optical enhancement of Au doped ZrO_2 thin films by sol–gel dip coating method, Phys. B Condens. Matter 457 (2015) 182–187.
[55] Y.S. Vidya, K.S. Anantharaju, H. Nagabhushana, S.C. Sharma, H.P. Nagaswarup, S.C. Prashantha, C. Shivakumara, Combustion synthesized tetragonal ZrO_2:Eu^{3+} nanophosphors: Structural and photoluminescence studies, Spectrochimica Acta Part A Mol. Biomol. Spectrosc. 135 (2015) 241–251.
[56] J. Berlin, S.S. Lekshmy, V. Ganesan, P.V. Thomas, K. Joy, Effect of Mn doping on the structural and optical properties of ZrO_2 thin films prepared by sol–gel method, Thin Solid Films 550 (2014) 199–205.
[57] R.H. French, S.J. Glass, F.S. Ochuchi, Y.-N. Xu, W.Y. Ching, Experimental and theoretical determination of the electron structure and optical properties of three phases of ZrO_2, Phys. Rev. B Condens. Matter 49 (1994) 5133–5142.
[58] D.W. Mc Comb, Bonding and electronic structure in zirconia pseudopolymorphs investigated by electron energy-loss spectroscopy, Phys. Rev. B 54 (1996) 7094–7102.
[59] J. Wang, Y. Xu, M. Hojamberdiev, Y. Cui, H. Liu, G. Zhu, Optical properties of porous YVO_4:Ln (Ln= Dy^{3+} and Tm^{3+}) nanoplates obtained by the chemical co-precipitation method, J. Alloys Compd. 479 (2009) 772–776.
[60] Y. Xie, Z. Ma, L. Liu, Y. Su, H. Zhao, Y. Liu, Z. Hang, H. Duan, J.Liand, E. Xie, Oxygen defects-modulated green photoluminescence of Tb-doped ZrO_2 nanofibers, Appl. Phys. Lett. 97 (2010) 141916.
[61] L. Chen, Y. Liu, Y. Li, Preparation and characterization of ZrO_2:Eu^{3+} phosphors, J. Alloys Compd. 381 (2004) 266.
[62] Y. Cong, B. Li, S. Yue, D. Fan, X.-J. Wang, Effect of Oxygen Vacancy on Phase Transition and Photoluminescence Properties of Nanocrystalline Zirconia Synthesized by the One-Pot Reaction, J. Phys. Chem. C 113 (2009) 13974.
[63] P. Iacconi, D. Lapraz, R. Caruba, Traps and emission centers in thermoluminescent ZrO_2, Phys. Status Solidi A 50 (1978) 275.
[64] J. Liang, Z. Deng, X. Jiang, F. Li, Y. Li, Photoluminescence of Tetragonal ZrO_2 Nanoparticles Synthesized by Microwave Irradiation, Inorg. Chem. 41 (2002) 3602.
[65] N. Salah, S.S. Habib, Z.H. Khan, F. Djouider, Thermoluminescence and photoluminescence of ZrO_2 nanoparticles, Phys. Chem. 80 (2011) 923.
[66] J.S. Lakshmi, I. John Berlin, G.P. Daniel, P.V. Thomas, K. Joy, Effect of calcination atmosphere on photoluminescence properties of nanocrystalline ZrO_2 thin films prepared by sol–gel dip coating method, Phys. B 406 (2011) 3050.
[67] A.A. Benyagoub, Mechanism of the monoclinic-to-tetragonal phase transition induced in zirconia and hafnia by swift heavy ions, Phys. Rev. B 72 (2005) 094114.
[68] Z. Wang, et al., The unusual variations of photoluminescence and afterglow properties in monoclinic ZrO_2 by annealing,, J. Luminescence 132 (2012) 2817–2821.
[69] E.W. Barrera, C. Cascales, M.C. Pujo, K.H. Park, S.B. Choi, F. Rotermund, J.J. Carvajal, X. Mateos, M. Aguiló, F. Díaz, Synthesis of Tm:Lu_2O_3 nanocrystals for phosphor blue applications, Phys. Procedia 8 (2010) 142–150.
[70] M.A. Zaitoun, S. Al-Tarawneh, Effect of the local coordination sphereon luminescence of inorganic and organic lanthanide-complexes encapsulated in sol-gel host glasses, J. Lumin 131 (2011) 1795.
[71] T.K. Anh, N.D. Hung, N.H. Chi, N.M. Son, Energy Transfer between Tb^{3+} and Eu^{3+} in Rare Earth Pentaphosphates, Phys. status solidi (a) 84 (1984) K159–K163.
[72] M. Back, M. Boffelli, A. Massari, R. Marin, F. Enrichi, P. Riello, Energy transfer between Tb^{3+} and Eu^{3+} in co-doped Y_2O_3 nanocrystals prepared by Pechini method, J. Nanopart Res. 15 (2013) 1753.